The Journal of Green Energy and Environmental Engineering

Research Paper

Synergistic Co-pyrolysis of Lignin and Cellulose for Fabricating Porous Carbon Applied in Supercapacitors

Anders Barton[1], Sunil Tuyan[2], Laurent Resin[1,*]

[1] Department of Civil Engineering, Eng. Faculty, Dokuz Eylül University, Buca-İzmir, Turkey
[2] Building Technology, School of Housing, Building and Planning, Universiti Sains Malaysia, 11800 Penang, Malaysia
*Corresponding author: laurentresin@deu.edu.tr

Abstract. Using enzymatic hydrolysis lignin and cellulose-containing waste textiles as co-precursors, with lignin and cellulose serving as composite carbon sources, porous carbon (TLPC) with a high specific surface area for supercapacitor applications was successfully prepared via a one-step carbonization-activation method. The microporous structure and electrochemical performance of the TLPC samples were systematically investigated. The results showed that at a carbonization temperature of 800 °C, the prepared TLPC-800 exhibited a high specific capacitance of 275 F/g at a current density of 0.5 A/g. When assembled into a symmetrical supercapacitor, the device delivered an energy density of 13.54 Wh/kg at a power density of 325 W/kg. After 10,000 charge-discharge cycles, the capacitance retention rate reached nearly 99.6% with a coulombic efficiency of approximately 100%, indicating excellent cycling stability. Furthermore, the assembled large-volume flexible solid-state supercapacitor also demonstrated favorable electrochemical performance.

Keywords: *Lignin; Cellulose; Waste textiles; Porous carbon; Supercapacitors*

Received on 15 Feb 2023, Accepted on 15 April 2023, Published on 15 May 2023

1 Introduction

The worldwide energy provision continues to be predominantly dependent on conventional fossil fuel resources, notably petroleum and natural gas. Their combustion releases large amounts of greenhouse gases, continuously exacerbating global warming and triggering various extreme environmental issues. Under the strategic background of "carbon peak" and "carbon neutrality," reducing dependence on fossil energy and promoting the transition to a clean and low-carbon energy structure has become a global consensus and a core development direction. Among various new energy technologies, supercapacitors, as a novel energy storage technology, integrate the advantages of traditional capacitors and batteries. These systems are distinguished by their capability for expedited energy storage and delivery, elevated power output, and extended operational lifespan, thereby garnering considerable research and commercial interest. In recent years, supercapacitors have found extensive deployment across portable consumer electronics, propulsion systems for alternative-energy automobiles, and sustainable power generation infrastructures.The judicious choice of electrode constituents plays a decisive role in governing supercapacitor performance. Porous carbonaceous materials synthesized from renewable biomass precursors present compelling advantages including economic viability, sustainable sourcing, and tunable porous architectures, positioning them as highly attractive candidates for electrode applications.Among diverse biomass feedstocks, lignin stands out as a principal by-product generated by the pulp and paper manufacturing sector, with substantial annual production volumes yet currently subjected to considerably underexploited, low-value applications.Lignin, constituting a significant by-product of the pulp and paper manufacturing sector, has attracted considerable attention as a promising carbonaceous precursor owing to its substantial natural availability, inherent aromatic backbone, and elevated carbon content (generally ranging between 55-65%).Its cross-linked, three-dimensional polyphenolic structure is rich in aromatic rings, which provides a natural tendency to form a rigid carbon skeleton during pyrolysis, leading to higher carbon yields compared to cellulose (e.g., LPC-800 yield of 27% in the document). This inherent "hard carbon" character makes

it structurally robust. The document emphasizes that lignin's high carbon content and thermal stability make it an ideal precursor. The activation process for lignin follows similar chemical pathways as for cellulose but often leverages its different chemical structure. KOH activation is highly effective, as detailed in the mechanistic discussion: the KOH or K_2CO_3 reacts with the carbon matrix, with K^+ intercalation and gasification (by CO_2, H_2O) playing key roles in creating porosity. The document references work by Cai et al., who used a two-step hydrothermal and weak alkali activation method on enzymatic hydrolysis lignin to produce porous carbon with an ultra-high specific surface area. However, such multi-step processes can be complex. The one-step method described in the document simplifies production. A key finding from the study is that lignin-derived carbon (LPC-800) alone, while yielding more carbon, developed a lower specific surface area (864 m^2/g) compared to the composite counterpart. This suggests that while lignin provides excellent skeletal stability, its dense, cross-linked structure might require more aggressive activation or complementary agents to achieve optimally high surface area and hierarchical porosity. Research trends in lignin-derived carbons include heteroatom self-doping (from lignin's inherent O, N, S), co-activation strategies, and combining lignin with other biomass or synthetic polymers to engineer pore architectures specifically for high-rate supercapacitors or battery anodes. The document's synergistic approach, using lignin to provide a rigid framework and cellulose to contribute initial micropores and higher surface area, effectively addresses the individual limitations of each precursor, highlighting a strategic direction in biomass carbon material design. The lignin macromolecule possesses abundant aromatic ring moieties coupled with substantial carbonaceous composition, rendering it an exemplary feedstock for the fabrication of porous carbon materials. Cai and co-workers utilized a sequential approach combining hydrothermal processing with mild alkaline activation to synthesize porous carbon exhibiting exceptionally high specific surface area from enzymatically hydrolyzed lignin. While this material demonstrated outstanding electrochemical characteristics, its multi-stage synthetic protocol presents challenges for scalable manufacturing and practical implementation.

Cellulose, being the most plentiful natural biopolymer present on Earth, serves as a highly attractive renewable feedstock for the fabrication of porous carbonaceous materials,particularly suited for electrochemical energy storage devices such as supercapacitors.Its linear polymer structure composed of glucose units offers a relatively straightforward carbonization pathway. The principal advantage of cellulose stems from its elevated purity levels and substantial oxygen content,which enables self-activation processes and promotes the incorporation of oxygen-functionalized surface groups during thermal decomposition, thereby enhancing pseudocapacitive contributions.As indicated in the referenced document, waste textiles predominantly composed of cellulose (exceeding 95% purity) are identified as a promising high-grade carbon precursor, attributed to their elevated cellulose content and minimal impurity levels. However, a significant challenge consistently reported in the literature, and confirmed in the document, is the severe mass loss during the direct pyrolysis of pure cellulose, leading to very low carbon yields (often below 15%, as seen with the TPC-800 sample yielding only 11%). This low yield poses a major economic and practical barrier for large-scale application. To overcome this and enhance porosity, activation is essential. Common activators include KOH, K_2CO_3, and $ZnCl_2$. The document describes the use of K_2CO_3, which acts through a combination of physical and chemical activation: its decomposition produces CO_2 for physical pore expansion, while the generated K_2O reacts with carbon to create metallic K vapor, which intercalates and etches the carbon lattice to create micropores. Research by Liu et al. (as cited) demonstrates that porous carbon derived from waste cotton textiles can achieve a mesoporous structure and good performance. The resulting cellulose-derived carbons often exhibit relatively high specific surface areas, as seen with TPC-800 having 921 m^2/g, but their structural strength can be limited due to the lack of a rigid aromatic framework, potentially leading to less robust pore structures under harsh activation conditions. Therefore, contemporary research often focuses on combining cellulose with other precursors (like lignin) or employing templating methods to improve yield, tailor pore size distribution, and enhance mechanical stability for practical device integration.Cellulose-containing waste textiles represent a typical type of cellulose-based solid waste. They are not only produced in vast quantities but also pose significant processing challenges, becoming a new environmental burden. Such waste textiles feature high cellulose content (greater than 95%) and low impurity levels, making them a potential high-quality carbon source for high-value-added carbon materials. Liu et al. used discarded natural cotton products as raw materials to prepare heteroatom-doped porous carbon with a mesoporous structure, which demonstrated good performance in supercapacitors. However, these waste textiles suffer from severe mass loss during pyrolysis, resulting in a low carbon yield (typically less than 15%), which severely limits their practical application as a carbon source for porous carbon preparation.

Building upon this foundation, the present investigation centers on the synergistic valorization of waste materialsIt utilizes spent enzymatic hydrolysis lignin derived from the pulp and paper sector alongside cellulose-rich waste textiles as dual carbon precursors,wherein the lignin and cellulose components function as integrated carbon sources, with potassium carbonate employed as an environmentally friendly activating agent. High-performance porous carbon is constructed in a structurally complementary manner through a one-step carbonization-activation method. The core of this research is to verify the effectiveness of the strategy for constructing high-performance porous carbon using lignin-cellulose composite carbon sources. By leveraging lignin to provide a rigid framework and cellulose to contribute initial micropores and a high specific surface area, the two complement each other structurally, overcoming the bottlenecks of single carbon sources, thereby achieving the construction of high-performance porous carbon. Building upon these findings, the present investigation systematically examines how variations in pyrolysis temperature affect the evolution of porous architecture and the resultant electrochemical behavior of the derived carbon materials. The investigation further characterizes the physicochemical attributes of porous carbon specimens synthesized under optimized conditions, and subsequently fabricates symmetric electrochemical capacitors together with flexible solid-state devices to comprehensively assess the energy storage capabilities of these carbonaceous materials. This research endeavor seeks to furnish innovative approaches for the valorization of lignocellulosic waste residues and the advancement of environmentally benign energy storage technologies.

2 Materials and Methods

2.1 Experimental Materials and Reagents

The waste textile materials were initially subjected to multiple washing cycles using deionized water and absolute ethanol, subsequently sectioned into cellulose-containing fragments with dimensions below 1 cm in both length and width. Commercial battery separator NKK-MPF30 was from NOK Corporation, Japan. Potassium hydroxide (KOH), wnzymatic hydrolysis lignin, polyacrylic acid-based hydrogel, anhydrous potassium carbonate (K_2CO_3), concentrated hydrochloric acid (HCl, mass fraction 36%), acetylene black, polytetrafluoroethylene, and anhydrous ethanol, all analytical grade, were purchased from Sigma Aldrich. 1 mol/L $TEABF_4$/PC electrolyte, platinum sheet electrode (10 mm length × 10 mm width × 0.1 mm thickness), and Hg/HgO electrode (filled internally with saturated potassium chloride solution) were purchased from Duoduo Chemical Reagent Co., Ltd. High-purity nickel foam was purchased from Kuma New Material Co., Ltd. Deionized water was prepared in the laboratory.

2.2 Experimental Methods

2.2.1 Preparation of Porous Carbon

A mixture comprising 1 g of enzymatically hydrolyzed lignin and 1 g of discarded textile material was dispersed in 50 mL of deionized water, to which 4 g of potassium carbonate was subsequently introduced, and the resulting suspension was agitated at ambient temperature for a duration of 60 minutes. The resulting blend was transferred into a vacuum desiccator maintained at 110 °C and subjected to exhaustive dehydration until complete dryness was attained. The dried precursor was subsequently positioned within a horizontal tubular furnace (Model OTF-1200X, Hefei Kejing Materials Technology Co., Ltd.), through which a continuous nitrogen flow (150 mL/min) was introduced. A controlled thermal ramp of 5 °C/min was applied, with isothermal maintenance for 60 minutes at target pyrolysis temperatures of 700, 800, and 900 °C, respectively. After allowing passive cooling to reach ambient temperature,the carbonized product was collected and sequentially washed with deionized water and 1 M hydrochloric acid until the resulting filtrate reached neutral pH. The solid residue was then transferred to a vacuum oven and dried at 80 °C for 12 hours, followed by comprehensive grinding to yield a series of porous carbon materials synthesized from enzymatic hydrolysis lignin and cellulose-rich waste textiles as dual precursors (designated as lignin-cellulose composite carbon sources). These were named TLPC-700, TLPC-800, and TLPC-900, respectively; where T represents cellulose, L represents lignin, PC represents porous carbon, and the number indicates the carbonization temperature.

Using the same preparation method, only 2 g of enzymatic hydrolysis lignin was added as the precursor (i.e., lignin single carbon source), and the porous carbon prepared at a carbonization temperature of 800 °C was

named LPC-800. Only 2 g of cellulose-containing waste textiles were added as the precursor (i.e., cellulose single carbon source), and the porous carbon prepared at a carbonization temperature of 800 °C was named TPC-800.

2.2.2 Preparation of Porous Carbon Electrodes

The as-synthesized porous carbon was combined with acetylene carbon black (functioning as the conductive additive) and polytetrafluoroethylene suspension (serving as the binding agent) in an 8:1:1 mass proportion, and the mixture was dispersed in a minimal quantity of absolute ethanol. After thorough grinding until the ethanol evaporated, the mixture was rolled into a film. The film was transferred to a vacuum drying oven and subjected to drying at 80 °C for a duration of 24 hours to eliminate residual moisture and organic solvents. The dried film was cut into rectangles measuring 1.5 cm in length and 1 cm in width, weighed, and recorded. Then, it was pressed onto cleaned nickel foam under 10 MPa to obtain the porous carbon electrode.

2.2.3 Assembly Methods for Supercapacitors

2.2.3.1 Flexible Solid-State Supercapacitor

Two porous carbon electrodes of equal mass and size (2 cm × 2 cm) were used as working electrodes. Polyacrylic acid-based hydrogel soaked in 6 mol/L KOH solution for 12 hours was used as the battery separator. Assembly was performed in an air environment, and then the device was packaged in a sealed bag to obtain a flexible solid-state supercapacitor. Air exposure was minimized as much as possible, and the device was stored for future use.

2.2.3.2 Symmetrical Supercapacitor

Two porous carbon electrodes of equal mass and size (12 mm diameter) were used as working electrodes, 6 mol/L KOH solution as the electrolyte, and NKK-MPF30 (19 mm diameter) as the battery separator. Assembly was performed in air in the order of positive shell, positive electrode, battery separator, negative electrode, spacer, spring, and negative shell. The cell was sealed using a battery crimping machine to obtain a symmetrical supercapacitor, which was then stored for future use.

The fabricated supercapacitor device was allowed to equilibrate at room temperature for 12 hours, ensuring comprehensive electrolyte penetration and complete wetting of the electrode materials before conducting electrochemical measurements.

2.3 Characterization and Testing

2.3.1 Material Characterization

The thermal resilience of the specimens was evaluated employing a thermogravimetric apparatus (TG, NETZSCH, Germany, STA449F3). The structural features of the specimens were examined utilizing field emission scanning electron microscopy (FESEM, HITACHI, Japan, SU8100) alongside transmission electron microscopy (TEM, JEOL, Japan, JEM-F200). The specific surface area together with pore size distribution were assessed via N_2 adsorption-desorption measurements employing an automated surface area measurement system (Micromeritics, UK, ASAP2460). Graphitization degree, crystalline phase composition, surface elemental composition, and additional attributes were investigated employing Raman spectroscopy (Renishaw, UK, inVia Reflex), X-ray diffraction (XRD, Rigaku, Japan, UltimaIV), and X-ray photoelectron spectroscopy (XPS, Thermo Scientific, USA, K-Alpha).

2.3.2 Electrochemical Testing

The electrochemical characteristics of the specimens were evaluated under ambient temperature conditions utilizing a potentiostat/galvanostat system (model CS300X, Wuhan Corrtest Instruments Corp., Ltd.). A three-electrode setup was utilized, with the as-synthesized porous carbon electrode serving as the working electrode, a platinum foil as the counter electrode, and a Hg/HgO electrode as the reference electrode. Cyclic voltammetry (CV) and galvanostatic charge-discharge (GCD) measurements were conducted within a potential window of -1.0 to 0 V. For electrochemical impedance spectroscopy (EIS) characterization, an alternating voltage perturbation of 10 mV was employed, with the frequency range spanning from 0.01 Hz to 100 kHz. In the case of the two-electrode setup, CV and GCD assessments were undertaken within a 6 mol/L KOH aqueous electrolyte, operating

across a potential span of 0 to 1.0 V.The EIS testing method was the same as for the three-electrode system. Cycling performance tests were conducted on a battery testing system (model CT-4000, Shenzhen Neware Electronics Co., Ltd.).

2.3.3 Calculation of Electrochemical Performance

For the three-electrode system, the mass-specific capacitance of the electrode (C_m, F/g) is calculated according to Equation (1).

$$C_m = (I \cdot \Delta t) / (m \cdot V) \quad (1)$$

Where, I represents the current, A; Δt represents the discharge time, s; m represents the mass of active material on the working electrode, g; V represents the discharge voltage, V.

For the two-electrode system, the mass-specific capacitance of the entire device (C_s, F/g) is calculated according to Equation (2).

$$C_s = (I \cdot \Delta t) / (2m_0 \cdot V) \quad (2)$$

Where, I represents the current, A; Δt represents the discharge time, s; m_o is the mass of active material on a single working electrode, g; V represents the discharge voltage, V.

The energy density (E, Wh/kg) and power density (P, W/kg) of the supercapacitor are calculated according to Equations (3) and (4), respectively.

$$E = C(\Delta V)^2 / (3.6 \times 2) \quad (3)$$

$$P = 3600E / \Delta t \quad (4)$$

Where, C represents the mass-specific capacitance of the entire capacitor, F/g; ΔV represents the discharge voltage range, V; Δt represents the discharge time, s.

3 Results and Discussion

3.1 Physicochemical Property Characterization of Porous Carbon

3.1.1 Morphology Analysis of Porous Carbon

The microstructural features of porous carbon were acquired via field emission scanning electron microscopy. Panels (a) through (c) in Figure 1 illustrate the surface topography of TLPC-700, TLPC-800, and TLPC-900, respectively—materials synthesized from lignin-cellulose composite precursors subjected to varying pyrolysis temperatures of 700°C, 800°C, and 900°C. From Figures 1(a)-(c), it can be seen that as the carbonization temperature increases, the activation and etching effect of K_2CO_3 becomes more significant. Dense and interconnected pore structures appear on the rod-like and blocky skeletons of each sample. Figures 1(d) and 1(f) show the FESEM images of porous carbons prepared from single carbon sources. Comparing Figures 1(a)-(c) with Figures 1(d) and 1(f), it can be seen that the porous carbon sample prepared from cellulose-containing waste textiles as the precursor retains the elongated fibrous morphology of cellulose, and tiny pores formed by activator etching can be observed on the fibers. The porous carbon sample prepared from enzymatic hydrolysis lignin as the precursor exhibits an irregular block shape rich in etched pores. The aforementioned findings demonstrate that K_2CO_3, serving as an activating agent, effectively develops a hierarchical porous architecture across the surfaces of both carbon precursors concurrently, substantially enhancing the specific surface area of the resulting material,thereby creating favorable conditions for rapid ionic transport and efficient energy storage, and consequently establishing a robust structural basis for superior electrochemical performance.

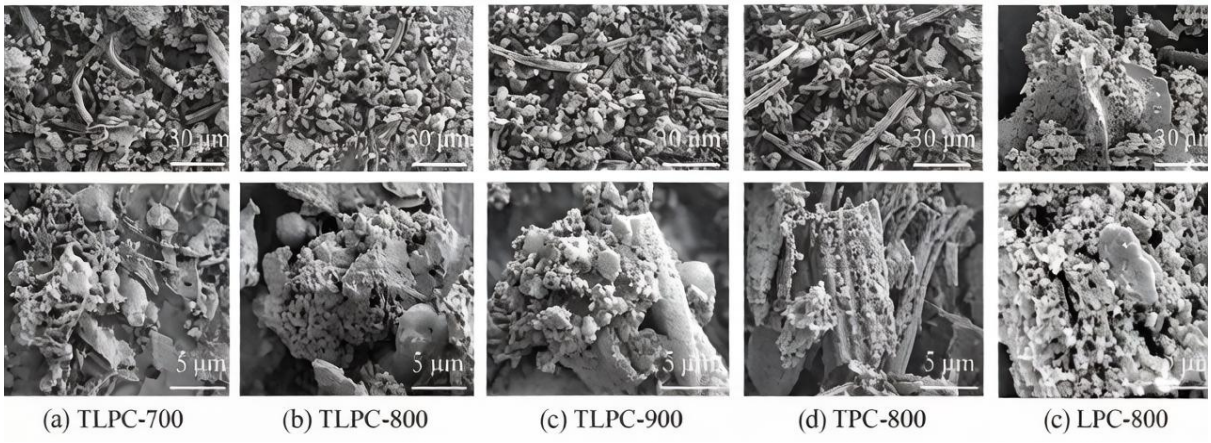

Figure 1 FESEM images of porous carbon samples

3.1.2 Pore Structure Analysis of Porous Carbon

Pore architecture represents a critical determinant governing the electrochemical behavior of carbon-based electrode materials.Illustrated in Figure 2 are the N_2 sorption isotherms together with the pore size distribution profiles corresponding to the porous carbon specimens.Figure 2(a) reveals that every porous carbon sample produced in this work displays pronounced nitrogen sorption at reduced pressures, which points toward well-developed microporosity throughout their framework. Additionally, porous carbons originating from lignin-cellulose hybrid feedstocks manifest superior nitrogen uptake relative to those manufactured from solitary carbon precursors. The pore size distribution profiles presented in Figure 2(b) provide additional confirmation that TLPC-800 possesses a porous architecture predominantly comprising micropores featuring diameters below 2 nm, accompanied by mesopores spanning the 2–5 nm range.The proportion of mesopores and macropores is about 30%. This hierarchical porous structure facilitates ion transport.

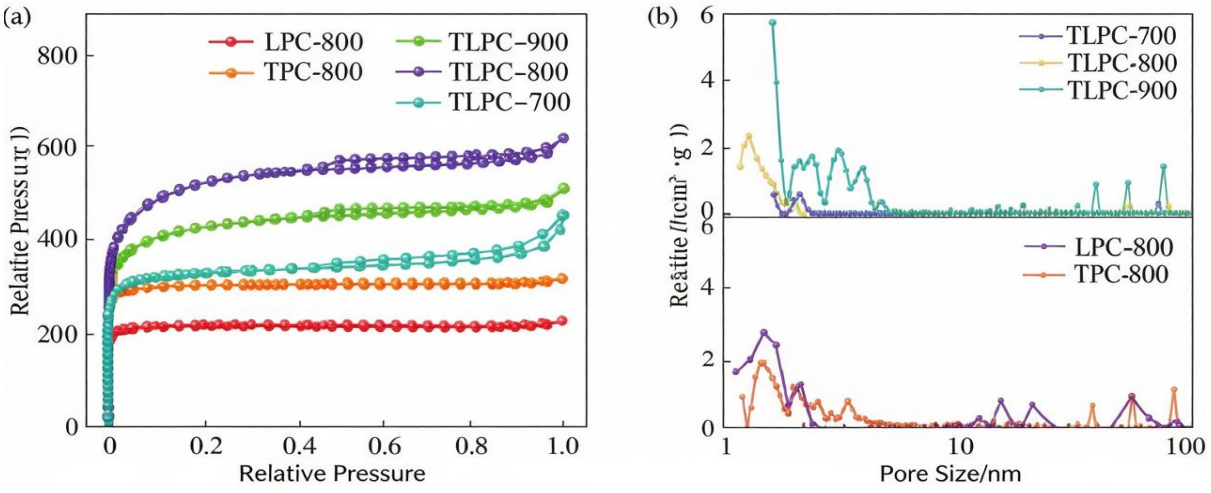

Figure 2 (a) N_2 adsorption-desorption curves, and (b) pore size distribution of porous carbon samples

Table 1 presents the specific surface area, pore volume, elemental composition, and production yield for the porous carbon specimens. As indicated in this table, TLPC-700, synthesized at a carbonization temperature of 700°C, exhibits a specific surface area of 1216 m^2/g. As the carbonization temperature is increased to 800°C, the specific surface area of TLPC-800 reaches 1554 m^2/g.This indicates that the activation and etching effect of K_2CO_3 is enhanced, leading to a rapid increase in specific surface area and total pore volume. This finding implies that K_2CO_3 exerts a more vigorous activating and corrosive influence at elevated temperatures, consequently accelerating the development of surface area and pore capacity. Nevertheless, when the carbonization

temperature advances to 900°C, the specific surface area of TLPC-900 contracts to 1313 m²/g. Therefore, there is an optimal activation temperature window for the preparation strategy using the lignin-cellulose composite carbon source. The specific surface area of LPC-800 prepared from the lignin single carbon source is only 864 m²/g, with a yield of 27%. The specific surface area of TPC-800 prepared from the cellulose single carbon source is 921 m²/g, but its yield is only 11%, indicating that cellulose suffers severe mass loss during carbonization and activation. This indicates that cellulose contributes to generating a higher specific surface area and a plentiful microporous architecture during the activation process, whereas lignin furnishes a robust carbon framework that mitigates carbon depletion throughout the pyrolytic process. The two synergize with each other, enabling the acquisition of a hierarchical pore structure under the premise of high yield, laying the foundation for subsequent electrochemical research.

Table 1 Specific surface area, pore volume, element and yield of porous carbon samples

Sample	Specific Surface Area / ($m^2 \cdot g^{-1}$)	Micropore Area / ($m^2 \cdot g^{-1}$)	Total Pore Volume / ($cm^3 \cdot g^{-1}$)	Average Pore Diameter / nm	Element Content / %			Yield / %
					C	O	N	
TLPC-700	1216	1150	0.789	1.608	92.00	6.29	1.72	23
TLPC-800	1554	1018	0.959	1.963	92.95	5.65	1.40	20
TLPC-900	1313	972	0.791	1.960	96.89	2.08	1.03	15
TPC-800	921	790	0.483	2.107	92.61	5.76	1.63	11
LPC-800	864	839	0.348	1.611	76.35	21.77	1.68	27

3.1.3 Chemical Structure Analysis of Porous Carbon

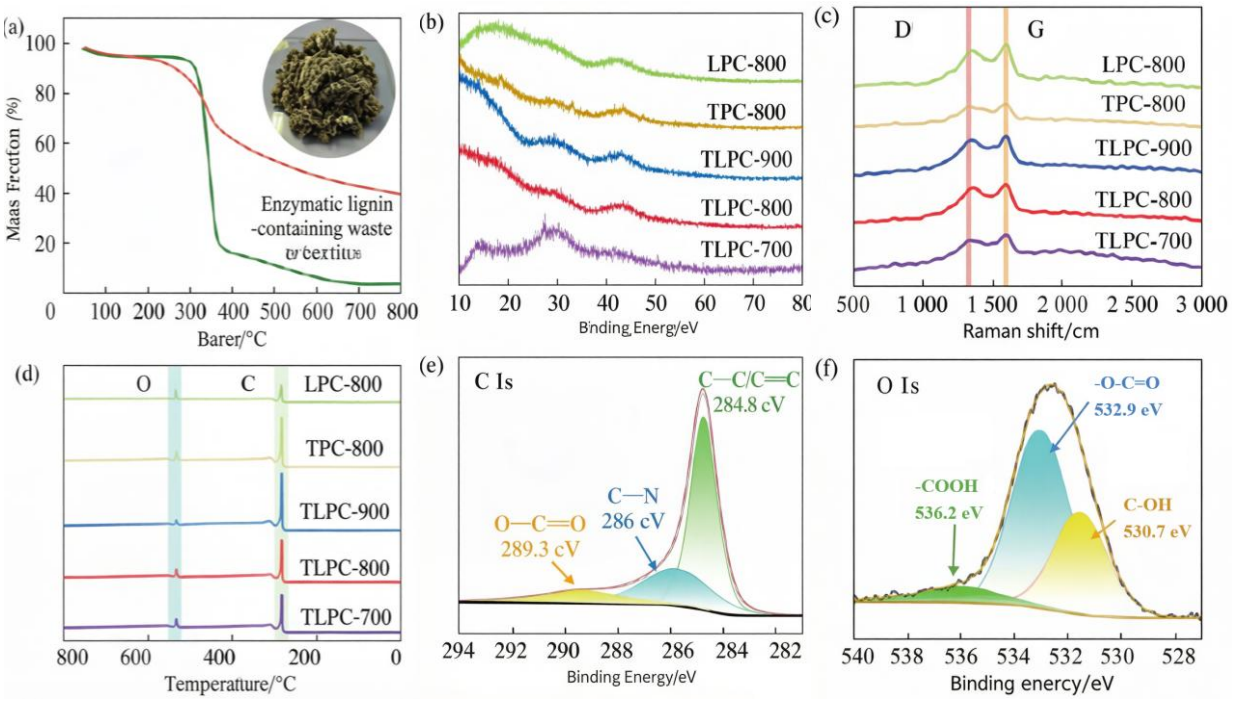

Figure 3 (a) TG curves, (b) XRD patterns, (c) Raman spectra, (d) XPS full spectra, (e) C 1s and (f) O 1s fine spectrum of TLPC-800

Thermal stability analysis was performed on enzymatic hydrolysis lignin and cellulose-containing waste textiles, and the results are shown in Figure 3(a). From Figure 3(a), it can be seen that cellulose-containing waste textiles begin to exhibit significant mass loss at about 350 °C, corresponding to chemical bond breakage and the release

of a large amount of volatile substances. This result indicates that K_2CO_3 demonstrates intensified activation and etching behavior as temperatures rise, thus promoting rapid growth in both surface area and total pore volume. Yet, upon pushing the carbonization temperature to 900°C, the specific surface area of TLPC-900 experiences a reduction to 1313 m^2/g.Among these specimens, TLPC-800 exhibits the maximum peak intensity, signifying the most pronounced graphitic ordering and consequently the optimal electrical conductivity.TLPC-800 demonstrates the greatest peak magnitude across all samples examined, which points toward the highest level of graphitic crystallinity and, by extension, superior charge transport properties. The D band corresponds to disordered or defective carbon structures, whereas the G band is associated with the well-ordered graphitic lattice.Based on peak intensity calculations, the I_D/I_G values for TLPC-700, TLPC-800, and TLPC-900 are 0.942, 0.928, and 0.911, respectively. This indicates that as the carbonization temperature increases, the proportion of graphite defect structures gradually decreases, and the degree of graphitization continuously increases. However, the lowest I_D/I_G value is still above 0.9, indicating that the prepared porous carbon contains abundant defect sites. These can serve as electrochemical active centers, contributing significant pseudocapacitance through reversible redox reactions or ion adsorption/desorption processes, thereby enhancing the overall electrochemical capacity of the supercapacitor.

The surface chemical properties of the porous carbon specimens were analyzed by X-ray photoelectron spectroscopy (XPS), with the corresponding results presented in Figures 3(d)-(f).The survey XPS spectra for all porous carbon samples (Figure 3(d)) exhibit intense C 1s signals along with distinct O 1s peaks, suggesting that the porous carbon materials are predominantly composed of carbon and oxygen elements. Figure 3(e) shows the high-resolution C 1s spectrum of TLPC-800. As shown in Figure 3(e), the C 1s peak of TLPC-800 can be fitted into three sub-peaks, attributed to C=C/C-C (284.8 eV), C-N (286 eV), and O-C=O (289.3 eV). Figure 3(f) shows the high-resolution O 1s spectrum of TLPC-800. As shown in Figure 3(f), the O 1s peak of TLPC-800 can be fitted into three sub-peaks, located at 531.7 eV, 532.9 eV, and 536.2 eV, attributed to C-OH, -O-C=O, and -COOH, respectively. These surface heteroatoms can not only enhance the wettability between the porous carbon and the electrolyte solution but can also undergo rapid Faraday reactions to provide partial pseudocapacitance. These characteristics operate in concert with the multiscale pore architecture, collectively enhancing the comprehensive energy storage capabilities of the supercapacitor device.

3.2 Analysis of Carbonization-Activation Mechanism

Drawing upon comprehensive structural elucidation of porous carbons derived from lignin-cellulose hybrid precursors, the integrated "simultaneous carbonization-activation" methodology can be delineated into three sequential phases.Stage I (150–400 °C): Differentiated pyrolysis of precursors and construction of the initial carbon skeleton and pores. Cellulose molecular chains first undergo dehydration reactions at 200–300 °C, removing intramolecular hydroxyl groups, generating H_2O and releasing it. At 300–400 °C, glycosidic bonds in the cellulose molecular chains break, decomposing into small molecular volatile components such as aldehydes and ketones. The violent release of these gaseous products leaves behind abundant initial micropores and ultra-micropores within the carbon matrix, creating the rudiments of a high specific surface area and channels for subsequent activator diffusion. However, the carbon skeleton is not yet cross-linked at this stage, and the structure is loose and prone to collapse. Lignin, as a rigid polymer, has a wider pyrolysis temperature range and higher thermal stability. In this stage, lignin mainly undergoes cleavage of side chains and ether bonds, but a large number of aromatic ring structures are preserved. This provides physical support, slowing down the overall structural collapse caused by the intense decomposition of cellulose, and begins to form preliminary cross-linked aromatic clusters, providing basic mechanical stability for the porous carbon.

Stage II (400–600 °C): Gas-solid synergy achieves physicochemical pore expansion. K_2CO_3 thermally decomposes to produce CO_2 (Equation (5)), serving as the main physical pore-forming agent. Its aggregation and escape within the carbon skeleton can expand micropores to form mesopores and enhance pore connectivity. The generated K_2O undergoes redox reactions with active carbon, producing metallic potassium (K) vapor and CO (Equation (6)). This reaction is the core step of chemical activation. The generated CO further etches the carbon skeleton, enlarging the pore volume, and can embed into the interlayers of fragile amorphous carbon microcrystals. Through an intercalation-etching effect, it widens some initial micropores and creates a large number of new micropores. Simultaneously, the generated CO can also act as a mild oxidant to further etch carbon walls, causing adjacent micropores to interconnect, forming a more open pore network. This process significantly increases the

micropore specific surface area and pore volume of the porous carbon.

$K_2CO_3 \rightarrow K_2O + CO_2\uparrow$ (5)

$K_2O + C \rightarrow K\uparrow + CO\uparrow$ (6)

Stage III (600–800 °C): K vapor intercalation and catalytic etching. 800 °C is close to the boiling point of metallic potassium, and the concentration of K vapor reaches its peak. It first intercalates into carbon layers to expand the interlayer spacing of carbon microcrystals. Following this, potassium vapor selectively promotes the corrosion of disordered carbon domains, thereby conserving aromatic ring moieties and generating a multilevel porous framework encompassing micropores, mesopores, and macropores.This achievement establishes a synergistic balance between considerable specific surface area and accelerated ion migration dynamics. As a result, the porous carbon maintains impressive specific capacitance alongside outstanding retention characteristics at elevated current densities, satisfying the paired prerequisites of advanced supercapacitor systems for both energy density and power density performance.

3.3 Analysis on Electrochemical Performance

The electrochemical characteristics of the porous carbon specimens were assessed through measurements conducted in a three-electrode configuration employing 6 M KOH as the electrolyte. Figure 4(a) shows that the porous carbon samples had CV curves at a scan rate of 20 mV/s. From Figure 4(a), it can be seen that the cyclic voltammetry curves of all porous carbon samples exhibit a quasi-rectangular shape, indicating that electric double-layer capacitance dominates. By comparison, TLPC-800 has the largest enclosed area under its cyclic voltammetry curve, indicating the greatest performance. Figure 4(b) exhibited the galvanostatic charge-discharge profiles for all porous carbon samples recorded at a current density of 1 A/g .As found in Figure 4(b), the galvanostatic charge-discharge profiles for every porous carbon specimen display nearly symmetric triangular shapes, which attests to the favorable electrochemical reversibility inherent in all synthesized porous carbon materials. Panels 4(c) and 4(d) additionally present the cyclic voltammetry responses of TLPC-800 recorded at elevated potential sweep rates, together with its galvanostatic charge-discharge characteristics measured under varying current densities. As evidenced in Figures 4(c) and 4(d), the cyclic voltammetry profile of TLPC-800 retains a quasi-rectangular geometry even when subjected to an exceptionally high sweep rate of 100 mV/s, thereby attesting to its superior rate capability. Moreover, the galvanostatic charge-discharge traces recorded across diverse current densities all display pronounced symmetry with minimal IR drop, signifying excellent charge-discharge reversibility.

Depicted in Figure 4(e) are the Nyquist plots for all porous carbon samples examined. A diminished Rct value signifies reduced charge transfer impedance at the electrode-electrolyte boundary, thereby facilitating more rapid redox kinetics, attenuated polarization phenomena, and enhanced performance under elevated discharge rates. The inclined line approximating 45° within the low-frequency domain corresponds to Warburg diffusion resistance. Meanwhile, a vertical alignment approaching the imaginary axis at low frequencies signifies near-ideal capacitive characteristics. As revealed in Figure 4(e), TLPC-800 exhibits the minimal real-axis intercept coupled with the smallest semicircular arc diameter, collectively indicating the lowest overall impedance among all samples evaluated. This phenomenon may be ascribed to the cooperative interplay between its multiscale porous architecture and surface-bound oxygen functionalities. Displayed in Figure 4(f) are the specific capacitance magnitudes pertaining to diverse porous carbon samples investigated. Computed from the galvanostatic discharge characteristics illustrated herein, the gravimetric capacitances at 1 A/g current density are determined to be 224, 252, 201, 172, and 148 F/g for TLPC-700, TLPC-800, TLPC-900, LPC-800, and TPC-800, correspondingly. Additionally, the gravimetric capacitance of TLPC-800 attained at a reduced current density of 0.5 A/g at a value of 275 F/g. This fully demonstrates that its optimized micropore/mesopore distribution and defect sites can endow it with excellent supercapacitor performance.

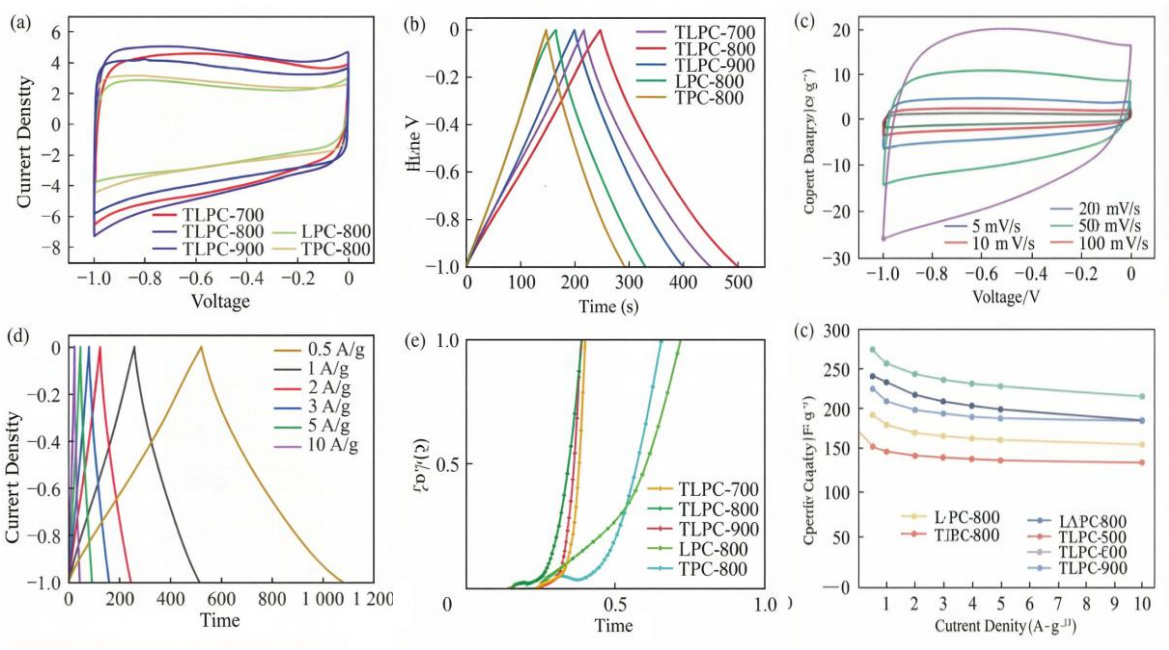

Figure 4 (a) cyclic voltammetry curves and (b) galvanostatic charge-discharge curves of the porous carbon samples, (c) cyclic voltammetry curves and (d) galvanostatic charge-discharge curves of TLPC-800, (e) electrochemical impedance spectroscopy curves, (f) specific capacitance at different current densities

Additionally, a polyacrylic acid-based hydrogel saturated in 6 M KOH electrolyte was employed as separator membrane,and TLPC-800 was fabricated into a large-scale flexible solid-state supercapacitor device, with its electrochemical performance subsequently evaluated, as illustrated in Figure 5(a).

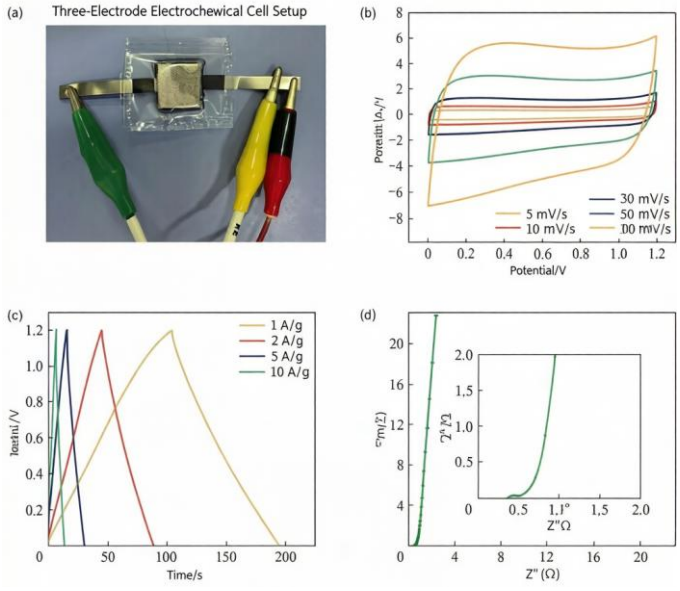

Figure 5 (a) Schematic diagram, (b) CV curves, (c) EIS curves, (d) GCD curve of the assembled TLPC-800 flexible solid-state supercapacitor

Figure 5(b) displays the cyclic voltammograms of the TLPC-800-based flexible solid-state supercapacitor recorded within a potential window of 0–1.2 V. As evident from Figure 5(b),the CV profiles across scan rates ranging from 5 to 100 mV/s all demonstrate near-rectangular morphologies, indicative of the electric double-layer capacitive

characteristics of TLPC-800.Even at 100 mV/s, the CV curve shows no significant distortion, indicating that TLPC-800 can rapidly establish an electric double layer in the solid-state system and possesses efficient electron/ion transport capabilities. Figure 5(c) shows the EIS curve of the TLPC-800 flexible solid-state supercapacitor. Presented in Figure 5(c), the TLPC-800 flexible solid-state supercapacitor displays an equivalent series resistance of 0.4 Ω accompanied by a charge transfer resistance of merely 0.1 Ω. These appreciably decreased resistance quantities signify enhanced charge carrier movement and distinguished electrical conductivity, qualities rooted in its arranged graphitic constitution together with the graded pore construction. Figure 5(d) depicts the galvanostatic charge-discharge response for this conformable arrangement. Perceptible from Figure 5(d), at a current density of 1 A/g, the charge-discharge profile exhibits distinct triangular symmetry with roughly equivalent charging and discharging timeframes, consequently verifying adequate coulombic efficiency for the TLPC-800 flexible solid-state supercapacitor. Derived computations establish a gravimetric capacitance of 37.5 F/g. Furthermore, this flexible energy storage implementation retains an energy density of 7.8 Wh/kg while functioning at a power density of 300 W/kg, accentuating its considerable promise for adoption in wearable and flexible electronic implementations.

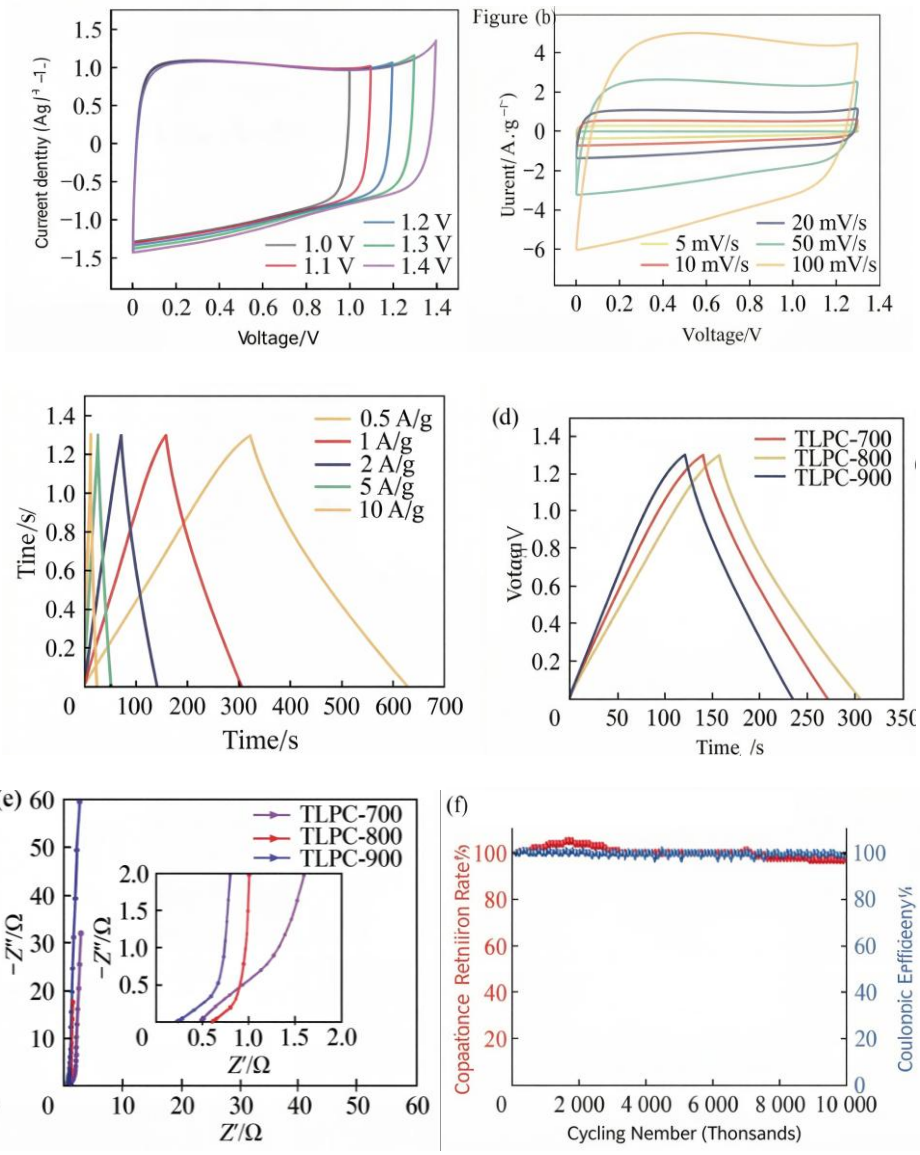

Figure 6 CV curves (a) under different voltage windows, and (b) at various scan rates, (c) GCD curves at different current densities of TLPC-800 coin-type supercapacitor, (d) GCD curves and (e) EIS curves of the porous carbon coin-type supercapacitor, (f) cycling stability of the TLPC-800 coin-type supercapacitor

To further investigate the application potential of TLPC-800 as a working electrode, it was assembled into a symmetrical supercapacitor, and its electrochemical performance was tested and analyzed. The cyclic voltammetry measurements compiled over assorted voltage intervals are rendered in Figure 6(a). Detectable from Figure 6(a), as the potential scope stretches from 1.0 V to 1.3 V, the CV silhouette for the TLPC-800 symmetric supercapacitor upholds a fundamentally rectangular geometry. Alternatively, upon forcing the voltage to 1.4 V, conspicuous aberration manifests in the CV trajectory of the TLPC-800 symmetric supercapacitor, suggesting electrolyte disintegration unfolding under such operational settings.Therefore, the stable voltage window for the TLPC-800 symmetrical supercapacitor in subsequent tests was set to 0–1.3 V. The cyclic voltammetry data compiled at assorted potential sweep rates are rendered in Figure 6(b). Discernible from Figure 6(b), across scan velocities spanning 5 mV/s to 100 mV/s, the CV trajectories for the TLPC-800 symmetric supercapacitor unwaveringly sustain fundamentally rectangular geometries, thereby exposing its electric double-layer capacitive features. Figures 6(c) and 6(d) illustrate the galvanostatic charge-discharge responses for the TLPC-800 symmetric supercapacitor at various current densities, together with the GCD curves for TLPC-700, TLPC-800, and TLPC-900 symmetric supercapacitors, respectively. All such GCD profiles conform to nearly isosceles triangular shapes, attesting to remarkable electrochemical reversibility.The calculated gravimetric specific capacitance for the TLPC-800 symmetric supercapacitor reaches 57.7 F/g at 1 A/g, which substantially surpasses the performance of other investigated samples. Furthermore, Figure 6(e) shows the EIS curves of the TLPC-700, TLPC-800, and TLPC-900 symmetrical supercapacitors. As illustrated in Figure 6(e), the TLPC-800 symmetric supercapacitor exhibits the lowest values for both equivalent series resistance and charge transfer resistance,suggesting that its hierarchically porous architecture effectively minimizes internal resistance, consequently enhancing ion transport kinetics and electrical conductivity.Additionally, the TLPC-800 symmetric supercapacitor completed 10,000 continuous charge-discharge cycles at a current density of 5 A/g, with outcomes illustrated in Figure 6(f). Apparent from Figure 6(f), the TLPC-800 symmetric supercapacitor shows distinguished cycling longevity, securing a specific capacitance retention close to 99.6% combined with a coulombic efficiency of about 100%. Derived calculations confirm that the TLPC-800 symmetric supercapacitor can deliver an energy density of 13.54 Wh/kg while functioning at a power density of 325 W/kg.

3.3 Mechanisms for enhanced properties of supercapacitor

Based on the detailed content provided in the document, the superior electrochemical performance of the lignin-cellulose co-derived porous carbon (TLPC), particularly the TLPC-800 sample, can be mechanistically attributed to the synergistic creation of an optimized hierarchical pore structure and a favorable surface chemical state, both resulting from the complementary roles of the two biomass precursors during the one-step K_2CO_3 activation process.

The most critical performance enhancement mechanism stems from the ideally constructed hierarchical pore architecture. Cellulose, with its linear polymer structure, undergoes severe decomposition and release of volatile gases (e.g., H_2O, aldehydes, ketones) at 300–400 °C. This violent gas evolution acts as an in-situ physical activator, creating abundant initial micropores and ultra-micropores within the forming carbon matrix, thereby laying the foundation for a high specific surface area. However, a carbon skeleton derived from cellulose alone is structurally weak and prone to collapse, leading to low carbon yield (11% for TPC-800). Herein lies the pivotal role of lignin. Its thermally stable, cross-linked aromatic structure provides a rigid skeletal framework that physically supports the structure, mitigates overall collapse during cellulose's intense decomposition, and results in a higher carbon yield (27% for LPC-800). More importantly, during the subsequent chemical activation stage (400–800 °C), K_2CO_3 decomposes and reacts via: $K_2CO_3 \rightarrow K_2O + CO_2$ and $K_2O + C \rightarrow K\uparrow + CO\uparrow$. The released CO_2 and CO gases further etch the carbon, while the metallic potassium (K) vapor intercalates into the carbon layers. The K vapor preferentially catalyzes the etching of amorphous regions, expanding micropores into mesopores and creating interconnection between pores. The synergy is clear: the initial micropores from cellulose provide channels for K vapor and gas diffusion, while the rigid lignin skeleton withstands the intense etching, preventing pore wall collapse. This synergistic interplay culminates in TLPC-800 attaining an elevated specific surface area of 1554 m^2/g alongside a cumulative pore volume of 0.959 cm^3/g, featuring an advantageous distribution encompassing micropores below 2 nm and mesopores within the 2–5 nm range accounting for approximately 30% of the total porosity. This hierarchical structure is fundamental for performance: micropores provide enormous surface area for ion adsorption (electric double-layer capacitance, EDLC), while interconnected mesopores serve as low-resistance ion highways, ensuring rapid ion transport to the micropore interiors even at

high current densities, thus enabling both high capacitance and excellent rate capability (Fig. 7).

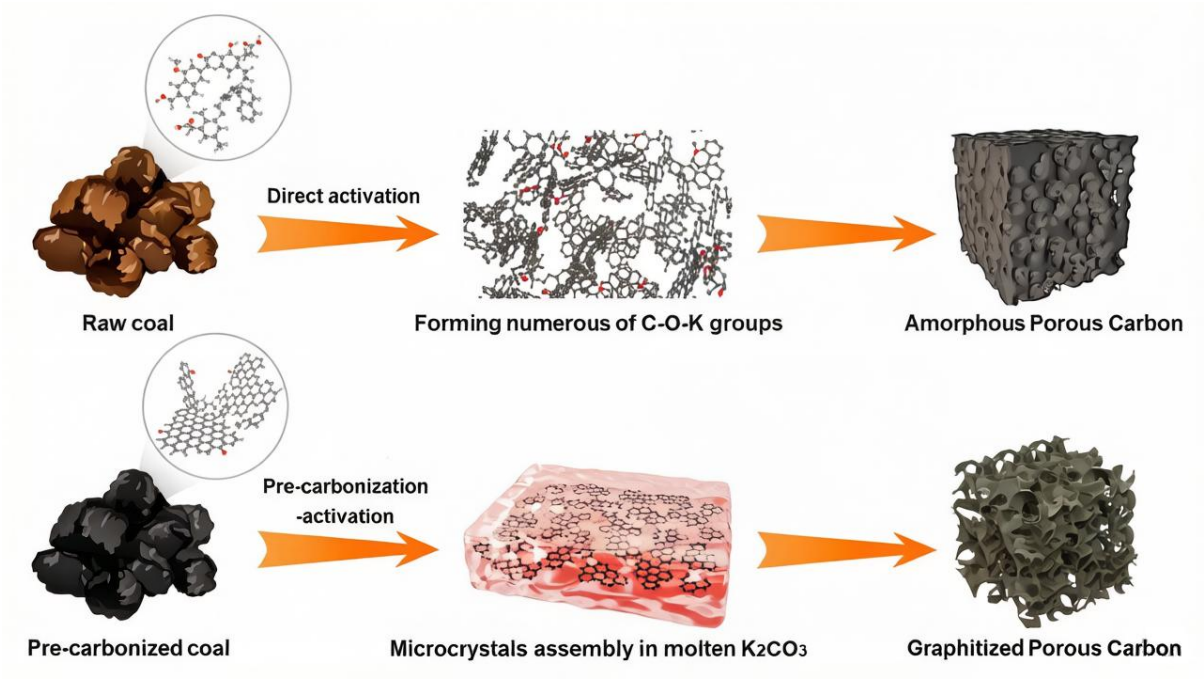

Figure 7 Mechanisms for enhanced properties of supercapacitor

Concurrently, the material's surface chemistry and structural order contribute significantly to the overall capacitance and conductivity. X-ray photoelectron spectroscopy (XPS) characterization verifies the existence of oxygen-functionalized surface groups, including hydroxyl (C-OH), ester (-O-C=O), and carboxyl (-COOH) moieties, on the carbon surface. These heteroatomic functionalities improve the electrode's wetting characteristics in aqueous KOH electrolyte, promoting comprehensive electrolyte penetration and access to the internal pore surfaces. Furthermore, these functional groups can undergo fast, reversible Faradaic redox reactions, providing an additional pseudo capacitance that supplements the primary EDLC. Raman spectroscopy reveals a moderate graphitization degree, as indicated by the I_D/I_G ratio of 0.928 for TLPC-800. While this signifies the presence of defect sites (beneficial for charge storage), the ordered graphitic domains (G-band) ensure good electronic conductivity throughout the carbon matrix. This cooperative interaction ultimately yields TLPC-800 with a substantial specific surface area of 1554 m^2/g and an aggregate pore volume of 0.959 cm^3/g, characterized by a favorable pore configuration comprising micropores smaller than 2 nm and mesopores spanning 2–5 nm that constitute roughly 30% of the overall porous network. The low Rct is a direct consequence of the hierarchical pores reducing ion diffusion barriers and the good electronic conductivity facilitating charge transfer. The amalgamation of these determining factors—accelerated ionic transport enabled by mesoporous pathways, considerable ion-accessible surface area stemming from microporous regions, extra redox reactivity contributed by surface functional groups, and reduced electronic resistance—jointly elucidates the remarkable specific capacitance (275 F/g at 0.5 A/g in a three-electrode setup; 57.7 F/g for the symmetric device), considerable energy density (13.54 Wh/kg at 325 W/kg), and distinguished cycling stability (99.6% retention after 10,000 cycles). The stability itself is inherent to the robust carbon skeleton derived from lignin and the primarily physical EDLC storage mechanism, which avoids the structural degradation associated with phase changes in battery materials.

Based on the two distinct technological pathways illustrated in the diagram—"Direct activation" of raw coal yielding Amorphous Porous Carbon and "Pre-carbonization-activation" leading to Graphitized Porous Carbon—the future application prospects of coal-derived porous carbons are highly promising and strategically diverse, bifurcating according to their final tailored structure. The direct KOH activation of raw coal, which involves forming numerous C-O-K groups and results in a highly amorphous carbon matrix with a vast, disordered pore network, is ideally suited for applications demanding ultra-high surface area and abundant active sites. This

makes it with high power density and rapid ion adsorption/desorption are critical, and for environmental remediation as an advanced adsorbent for large-scale capture of pollutants (e.g., CO2, organic dyes, heavy metals) due to its cost-effectiveness and high uptake capacity. Conversely, the innovative pre-carbonization followed by activation in molten K2CO3, which facilitates the "microcrystals assembly" into a graphitized structure, opens a pathway to more sophisticated applications. This material combines a conductive, ordered graphitic framework with a well-defined porous architecture. It is therefore exceptionally suitable as a durable support material for catalysts in demanding electrochemical reactions (such as oxygen reduction in fuel cells or hydrogen evolution), where electrical conductivity and stability are paramount. Moreover, its structural attributes render it highly suitable for application as an anode material in potassium-ion or sodium-ion battery systems,where the ordered carbon layers can facilitate the intercalation and de-intercalation of larger alkali metal ions more effectively than purely amorphous carbons. The key future direction lies in the intelligent, application-driven selection and further optimization of these pathways. By precisely controlling the pre-carbonization conditions and the nature of the molten salt activator, the degree of graphitization, pore size distribution, and heteroatom doping can be finely tuned. This enables the targeted synthesis of functional carbons from coal, a vast and carbon-rich resource, transforming it from a fuel into a precursor for high-value, performance-critical materials essential for the advancement of clean energy storage, conversion technologies, and sustainable chemical processes, thereby contributing to a more circular carbon economy.

4 Conclusion

This study harnessed enzymatic hydrolysis lignin, a secondary product emanating from pulp and paper production operations, alongside cellulose-laden textile discards as paired starting materials, wherein the lignin and cellulose elements operated as unified carbon precursors, while potassium carbonate served as the activation medium. Porous carbon substances distinguished by considerable specific surface areas were effectively produced through a one-stage carbonization-activation protocol. These materials were used as working electrodes to assemble symmetrical supercapacitors and flexible solid-state supercapacitors.

The integrated carbonization-activation methodology enables the concurrent fabrication of porous carbon materials exhibiting elevated specific surface areas alongside hierarchically organized pore architectures through synergistic effects. In the pyrolysis process using lignin and cellulose as composite carbon sources, cellulose provides initial pore channel structures, and lignin provides a rigid skeleton. The two complement each other synergistically. The TLPC-800 material synthesized at a carbonization temperature of 800 °C exhibits a remarkably high specific surface area of 1554 m^2/g coupled with a total pore volume of 0.959 cm^3/g.The hierarchically porous architecture facilitates enhanced transport efficiency for both ions and electrolyte within the porous carbon material.Operating within a three-electrode system employing 6 mol/L KOH electrolyte, the TLPC-800 electrode secured a specific capacitance of 252 F/g at a current density of 1 A/g. The constructed TLPC-800 symmetric supercapacitor furnished an energy density of 13.54 Wh/kg while functioning at a power density of 325 W/kg. After completing 10,000 charge-discharge cycles at 5 A/g, the device displayed a specific capacitance retention of 99.6% together with a coulombic efficiency of approximately 100%.Utilizing a polyacrylic acid-based hydrogel functioning as the electrolytic membrane, the constructed TLPC-800 flexible solid-state supercapacitor exhibited an equivalent series resistance of merely 0.4 Ω together with a charge transfer resistance of 0.1 Ω, denoting superior ion and electron transport properties combined with mechanical adaptability, thereby implying substantial applicability potential within the flexible energy storage domain.

References

[1] ASHOKKUMAR V, KUMAR G, LAKSHMANAN H, et al. A Critical Review of Biogas Production and Upgrading from Organic Wastes: Recent Advances, Challenges and Opportunities[J]. Biomass and Bioenergy, DOI: 10.1016/j.biombioe.2024.107566.

[2] HU X, LIU X, LI B, et al. Research Progress on Nickel-based Materials in Supercapacitors: A Review of Electrode Materials and Device Properties[J]. Small, DOI: 10.1002/small.202512830.

[3] TIAN Y, YUAN Y, SHEN Q, et al. Iron Oxide Quantum Dots-modified Biomass Carbon: Enabling High-performance Supercapacitors[J]. Advanced Sustainable Systems, DOI: 10.1002/adsu.202500624.

[4] ANJANA P M, AMINABHAVI T M. Supercapattery: Energy Storage Devices Combining Functionalities of

Battery Electrodes and Supercapacitor Electrodes[J]. Journal of Energy Storage, DOI: 10.1016/j.est.2025.118265.

[5] RADHAKRISHNAN K, KUMAR A. Advances and Challenges in Biomass-derived Supercapacitors[J]. Renewable and Sustainable Energy Reviews, DOI: 10.1016/j.rser.2025.116624.

[6] ZHANG D Y, QIAO Y C, SI C L, et al. Research Progress on the Preparation of Lignin-based Hard Carbon Materials and Their Applications in Sodium Ion Batteries[J]. Transactions of China Pulp and Paper, 2025, 40(3): 106–120.

[7] JHA S, MEHTA S, CHEN Y, et al. Design and Synthesis of Lignin-based Flexible Supercapacitors[J]. ACS Sustainable Chemistry & Engineering, 2019, 8(1): 498–511.

[8] CAI Z, QIU X, FU F, et al. Preparation of Nitrogen-doped Lignin Porous Carbon Using Low Dosage KHCO3 for Efficient Methylene Blue Adsorption: Activation Mechanism and Adsorption Performance[J]. International Journal of Biological Macromolecules, DOI: 10.1016/j.ijbiomac.2024.138319.

[9] WEI J S, DAI L, HE P, et al. Ultrathin and Flexible MXene-Contained Electromagnetic Interference Shielding Composite Paper Designed with a Protective Hydrogel Film[J]. Journal of Materials Science & Technology, 2024, 169: 199–208.

[10] LIU D, XU G, YUAN X, et al. Pore Size Distribution Modulation of Waste Cotton-derived Carbon Materials via Citrate Activator to Boost Supercapacitive Performance[J]. Fuel, DOI: 10.1016/j.fuel.2022.126044.

[11] WU Q, JIA Y, LIU Q, et al. Ultra-dense Carbon Defects as Highly Active Sites for Oxygen Reduction Catalysis[J]. Chem, 2022(8): 1–19.

[12] LI W, WAND G, SUI W, et al. Facile and Scalable Preparation of Cage-like Mesoporous Carbon from Lignin-based Phenolic Resin and its Application in Supercapacitor Electrodes[J]. Carbon, 2022, 196: 819–827.

[13] ZHANG C, CHEN Y S, YUAN C Y, et al. Research Progress on the Modification of Lignin-based Carbon Materials and Their Application in Supercapacitors[J]. China Pulp & Paper, 2024, 43(9): 20–30.

[14] SUN Y K, XU D, WANG S R. Self-assembly of Biomass Derivatives into Multiple Heteroatom-doped 3D-Interconnected Porous Carbon for Advanced Supercapacitors[J]. Carbon, 2022, 199: 258–267.

[15] HE W, LI H, LONG B, et al. One-step Synthesis of ZnNCN Nanoparticles with Adjustable Composition for an Advanced Anode in Lithium Ion Battery[J]. ACS Applied Energy Materials, 2021, 4(5): 4290–4296.

[16] ZHANG W, SUN M, YIN J, et al. Rational Design of Carbon Anodes by Catalytic Pyrolysis of Graphitic Carbon Nitride for Efficient Storage of Na and K Mobile Ions[J]. Nano Energy, DOI: 10.1016/j.nanoen.2021.106184.

[17] WANG Y, WANG H, ZHANG T C, et al. N-doped Porous Carbon Derived from rGO-incorporated Polyphenylenediamine Composites for CO2 Adsorption and Supercapacitors[J]. Journal of Power Sources, DOI: 10.1016/j.jpowsour.2020.228610.

[18] ZHANG H C, LI C Y, SUN R C, et al. Lignin-derived N, B, and F Tri-doped Carbon Fibers for Improving Electrochemical Performances of Lithium-Sulfur Battery Separators[J]. Transactions of China Pulp and Paper, 2025, 40(4): 20–30.

[19] CAI T X, YANG Z Y, LIU J D, et al. Carboxymethyl Chitosan-derived Carbon Foam with Hierarchical Pores Tuned by Potassium Tetraborate and Potassium Carbonate for Supercapacitors[J]. Journal of Energy Storage, DOI: 10.1016/j.est.2023.106671.

[20] MA T, XU S, ZHU M. Hierarchical Porous Carbon Based on Waste Quinoa Straw for High-performance Supercapacitors[J]. ACS Omega, 2024, 9(12): 13592–13602.

[21] LOBATO P D R, AMARO R, ARIAS D M, et al. Activated Carbon from Wasp Hive for Aqueous Electrolyte Supercapacitor Application[J]. Journal of Electroanalytical Chemistry, DOI: 10.1016/j.jelechem.2021.115777.

[22] CHANG T Y, GURUSAMY L, KARUPPASAMY L, et al. Porous Carbon Derived from Rice Straw Combined with the Polyhedron Morphology of CoMn2NiO for Supercapacitor Application[J]. Materials Today Chemistry, DOI: 10.1016/j.mtchem.2025.103073.

[23] ZENG F E, YAND X, ZHANG Y N, et al. Lignin-based Carbon Materials with High Mesopore Rate for Symmetric Supercapacitors[J]. Materials Today Communications, DOI: 10.1016/j.mtcomm.2024.111431.

[24] DONG Y, ZHANG S, DU X, et al. Boosting the Electrical Double-layer Capacitance of Graphene by Self-doped Defects Through Ball-milling[J]. Advanced Functional Materials, DOI: 10.1002/adfm.201901127.

[25] TIAN H D, FANG Q Q, Cheng R R, et al. Molten Salt Template-Assisted Synthesis of N, S-codoped Hierarchically Porous Carbon Nanosheets for Efficient Energy Storage[J]. Colloids and Surfaces A: Physicochemical and Engineering Aspects, DOI: 10.1016/j.colsurfa.2021.126172.

[26] TONG Y, WU C, HE H Q, et al. Iron-assisted Molten Salt Synthesis of Highly Graphitized Hierarchical Porous N-doped Carbon for Enhanced Aqueous Energy Storage[J]. Journal of Power Sources, DOI:

10.1016/j.jpowsour.2025.237086.

[27] REN X L, LIU X Z, LIU W, et al. Preparation and Performance of Lignocellulose Based Carbon Material for Supercapacitor[J]. China Pulp & Paper, 2021, 40(10): 10–17.

[28] ZHAI S, LI K, LI C, et al. Lignin-derived N, S-codoped Hierarchical Porous Carbons with High Mesoporous Rate for Sustainable Supercapacitive Energy Storage[J]. Journal of Energy Storage, DOI: 10.1016/j.est.2024.111036.

[29] WANG B, ZONG Z, QIAO Y F, et al. Ultrafast Synthesis of Hierarchically Porous Carbon for Efficient Electrochemical Energy Storage via Electromagnetic Thermal Activation[J]. Journal of Energy Storage, DOI: 10.1016/j.est.2025.118024.